Triton Elastic Scattering*

J. C. HAFELE,† E. R. FLYNN, AND A. G. BLAIR‡
Los Alamos Scientific Laboratory, University of California, Los Alamos, New Mexico
(Received 24 October 1966)

Differential cross sections for 15- and 20-MeV tritons elastically scattered from ^{52}Cr and ^{62}Ni and 20-MeV tritons from ^{64}Ni, ^{90}Zr, and ^{116}Sn are reported. The data are in good agreement with optical-model calculations using standard Woods-Saxon potential wells. The derived optical parameters are considered useful in distorted-wave calculations for reactions involving tritons and also indicate physical features of the triton interaction.

I. INTRODUCTION

THE optical-model description of nuclear scattering, used successfully for many years for protons, neutrons, and ^{4}He ions, in recent years has been applied to more loosely bound and complex particles, such as deuterons and ^{3}He ions. The behavior of the interaction of these particles with nuclei is of interest for its own sake, but in addition, the wave functions generated by the optical potentials may be used in distorted-wave Born approximation (DWBA) calculations for nuclear reactions. In fact, at the present time, the successful application of the DWBA theory rests to a large degree on the use of suitable wave functions in the entrance and exit channels generated in this manner.[1]

One of the particles for which the knowledge of optical-model potentials would be very useful is the triton. Owing to the relative unavailability of triton beams, there have been very few optical-model studies for this particle. The triton-optical potentials used in DWBA calculations, e.g., for the (d,t) reaction, usually have been obtained from the potentials known for other particles. Recently, however, studies of triton elastic scattering and optical-model fits to the experimental angular distributions have been reported.[2] The attainment of a triton beam from the Los Alamos three-stage Van de Graaff accelerator provides another facility for triton scattering studies.

The present paper reports the results of elastic scattering of tritons from several nuclei, in some cases at two energies, and the results of optical-model fits to the angular distributions. This study is not intended in any way as a survey; in fact, nearly all of the data were taken in order to obtain optical-model parameters for use in DWBA calculations for reactions such as (t,t') and $(t,^4\mathrm{He})$. The present results can be regarded only as a guide to the optical-model behavior of tritons scattered from medium-mass nuclei. Furthermore, since angular distributions of elastically scattered unpolarized particles are rather insensitive to spin-orbit forces, the present study does not provide much information on the shape or magnitude of the $\boldsymbol{\sigma}\cdot\mathbf{L}$ term in the potential.

In the optical-model analysis of the data, discrete sets or families of parameter values were found which yield good fits to the data, and within each set there are ambiguities between the well depths and the radii. These effects also have been observed for other highly absorbed particles.[3] Although for the case of ^{62}Ni the results are presented for several discrete sets, attention has primarily focused on that set for which the real-well potential is in the neighborhood of 150 MeV, i.e., approximately three times the potential for protons or neutrons. Results are presented which were obtained by allowing most of the geometrical parameters to vary from nucleus to nucleus, and also results from specifying a common geometry for all the nuclei studied. Finally, results are presented from requiring equal values for the real and imaginary geometrical parameters.

II. EXPERIMENTAL METHOD

The triton beam for the work reported here was obtained from the Los Alamos three-stage Van de Graaff facility; beam energies of both 15 and 20 MeV were used. The particle beam from the accelerator was defined by a $\frac{5}{32}\times\frac{1}{16}$-in. vertical collimating slit, passed through the target under study which was located at the center of a 20-in.-diameter scattering chamber, and stopped in a distant Faraday cup where the charge was collected. The integrated current was determined to within $\pm 0.25\%$. A ΔE-E combination of silicon solid-state detectors was mounted on an arm that is precisely positioned around the target by means of a remotely controlled radar antenna drive. The relative angular setting was accurate to within ± 0.05 deg. Left-right elastic scattering measurements at several angles gave the zero-degree setting to within ± 0.1 deg. The angular resolution at forward angles ($\theta \leq 48°$) was approximately 0.25°, and at backward angles was approximately 0.5°.

The ΔE detector was of the transmission type, with a thickness of 500 μ and an area of 50 mm^2; the E counter was a lithium-drifted silicon unit with a depth of 3 mm and an area of 80 mm^2. In addition to the ΔE-E pair, a monitor detector was used which measured the elastically scattered intensity and indicated any changes

* Work performed under the auspices of the U. S. Atomic Energy Commission.
† Now at Washington University, St. Louis, Missouri.
‡ Presently on leave at Centre d'Etudes Nucléaires de Saclay, Gif-sur-Yvette, Seine et Oise, France.
[1] L. L. Lee, Jr., J. P. Schiffer, B. Zeidman, G. R. Satchler, R. M. Drisko, and R. H. Bassel, Phys. Rev. **136**, B971 (1964).
[2] R. N. Glover and A. D. W. Jones, Nucl. Phys. **81**, 268 (1966).
[3] R. M. Drisko, G. R. Satchler, and R. H. Bassel, Phys. Letters **5**, 347 (1963).

occurring in the beam or target characteristics during the experimental runs. This detector was mounted on another arm which was set on the side of the scattering chamber opposite to the remotely controlled arm. The monitor detector was a 500-μ surface-barrier unit, in front of which was placed a gold-foil absorber that sufficiently degraded the energy of the elastically scattered tritons so that they stopped in the detector.

Except for ^{90}Zr, the targets were metallic foils fabricated by vacuum evaporation. The ^{90}Zr target was a rolled foil supplied by Oak Ridge National Laboratory. All of the targets were of highly enriched isotopic composition. The areal densities for the different targets ranged from 150 to 600 μg/cm^2 with uncertainties of about $\pm 15\%$. Beam energy loss in the targets was of the order of 10 keV.

Signals from the ΔE and E detectors were fed to charge-sensitive preamplifiers and the resulting pulses were summed, amplified, and then fed to a 1024-channel Victoreen analog-to-digital converter (ADC). Simultaneously, an analog multiplier examined the ΔE and E pulses and provided mass identification so that pulses corresponding to particles of only the desired mass could be tagged and gated into the ADC. The digital information from the ADC was stored in and analyzed by an on-line SDS–930 computer.

The computer has numerous time-sharing features that permit some degree of data analysis without interruption of data acquisition. In particular, for this work, peak areas were extracted on-line with a least-squares program that fit the data peaks to skewed Gaussian functions. After each run, this program stored the computed results and the data on a magnetic tape, thereby simplifying further examination of the data with off-line computations. It was also possible to store the data from a previous run temporarily on another magnetic tape and apply the fitting routine to these data while simultaneously recording data from the succeeding run. Furthermore, upon command at any time during a run, a printed listing of the accumulated data could be obtained and, if also desired, a computation of the least-squares fit to the accumulated data could be performed. These operations all occurred on an interrupt basis without impeding the data-acquisition rate. Pulses from the monitor detector, from the beam-current integrator, and dead-time corrections from the ADC unit were also fed to the computer on an interrupt basis, and corrections for lost counts were automatically applied by the program.

The ability to perform a certain amount of on-line data processing had considerable advantages compared to off-line data processing. For example, certain equipment failures or changes in the experimental conditions which ordinarily would have remained undetected until later processing of the data became apparent with the immediately available fits to the pulse-height spectra. In addition, the on-line computations reduced considerably the length of time required for a complete reduction of the data. Besides providing final results for the elastic peak and many of the inelastic peaks, the analysis served as a guide for the final (off-line) analysis of other inelastic peaks.

III. EXPERIMENTAL RESULTS

The data were recorded in 3° angular intervals from a minimum angle of 10° to a maximum angle determined by the intensity of the elastically scattered tritons and the available running time. The resulting differential cross sections for the five isotopes studied are tabulated in Table I. Angular distributions for ^{52}Cr and ^{62}Ni were measured at incident energies of both 15 and 20 MeV and for the other nuclei at only 20 MeV. A sufficient count at each angle was accumulated to reduce the statistical uncertainty and therefore the relative uncertainty to less than $\pm 5\%$ for every cross section given in Table I. Although the absolute cross sections could not be directly calculated to better than $\pm 15\%$ because of uncertainties in the thickness of the targets, it was possible to reduce the absolute uncertainty to less than $\pm 5\%$ by use of the forward-angle data. For small angles at the energies used, the cross section is dominated by Rutherford scattering and is thus relatively insensitive to the optical-model parameters. Thus the absolute cross section was more accurately determined by renormalizing the angular distribution for each case until the forward angles were optimally fit. The appropriate renormalization factors have been applied to the cross sections given in Table I.

IV. OPTICAL-MODEL ANALYSIS

The computer code of Perey[4] was used to compare the data to the optical-model theory and to extract appropriate optical-model parameters. This code searches on those parameters that are preassigned as variables until a minimum in the value of χ^2 is obtained, where

$$\chi^2 \equiv \frac{1}{N} \sum_{i=1}^{N} \left[\frac{\sigma_{\text{th}}(\theta_i) - R\sigma_{\text{ex}}(\theta_i)}{\Delta\sigma_{\text{ex}}(\theta_i)} \right]^2. \quad (1)$$

The σ's refer to the cross-section values, and N is the number of experimental points included in the fit. All the $\Delta\sigma$'s were assigned a relative value of 5%. R is the renormalization factor mentioned in the previous section. Initially, optical-model parameters believed approximately correct were introduced into the calculation, the value of R was set to unity and the search was performed over the entire experimental angular distribution. The search was repeated for several values of R until that value was determined which yielded the optimum fit to the forward-angle data alone. As an example of the method, we list results for the 15-MeV

[4] F. G. Perey, Phys. Rev. **131**, 745 (1963).

TABLE I. Measured triton elastic-scattering cross sections versus angle. Angular distributions were measured for both 15- and 20-MeV incident triton energies for ^{52}Cr and ^{62}Ni; for ^{64}Ni, ^{90}Zr, and ^{116}Sn, they were measured at only 20 MeV.

^{52}Cr at 15 MeV		^{62}Ni at 15 MeV	
$\theta_{c.m.}$ (deg)	$(d\sigma/d\Omega)_{c.m.}$ (mb/sr)	$\theta_{c.m.}$ (deg)	$(d\sigma/d\Omega)_{c.m.}$ (mb/sr)
10.58	3.74×10^{4}	10.49	5.73×10^{4}
12.69	1.90×10^{4}	12.59	2.76×10^{4}
15.86	7.53×10^{3}	15.73	1.08×10^{4}
19.03	2.81×10^{3}	18.87	4.16×10^{3}
22.20	1.06×10^{3}	22.01	1.56×10^{3}
25.36	5.71×10^{2}	25.15	8.29×10^{2}
28.51	4.22×10^{2}	28.28	5.66×10^{2}
31.67	3.09×10^{2}	31.41	3.79×10^{2}
34.82	1.80×10^{2}	34.54	2.19×10^{2}
37.96	8.37×10	37.66	1.04×10^{2}
41.10	3.96×10	40.78	5.93×10
44.23	3.22×10	43.89	4.32×10
47.36	3.53×10	46.99	4.06×10
50.48	3.44×10	51.10	3.25×10
53.59	2.60×10	53.19	2.14×10
56.70	1.56×10	56.28	1.16×10
59.80	7.90	59.37	6.51
62.89	4.44	62.44	5.51
65.97	3.80	65.51	5.73
69.05	4.11	68.58	5.26
72.12	3.98	71.63	4.23
75.17	3.30	74.68	2.73
78.22	2.36	77.73	1.63
81.26	1.57	80.76	1.08
84.30	1.23	83.79	9.85×10^{-1}
87.32	1.09	86.81	1.04
90.33	9.21×10^{-1}	89.82	1.02
93.34	8.89×10^{-1}	92.82	7.48×10^{-1}
96.33	6.38×10^{-1}	95.82	5.70×10^{-1}
99.32	4.52×10^{-1}	98.81	3.70×10^{-1}
102.3	3.18×10^{-1}	101.8	2.62×10^{-1}
105.3	2.43×10^{-1}	104.8	2.24×10^{-1}
108.2	2.40×10^{-1}	107.7	2.11×10^{-1}
111.2	2.76×10^{-1}	110.7	2.20×10^{-1}
114.1	2.72×10^{-1}	113.6	1.88×10^{-1}
117.0	2.61×10^{-1}	116.6	1.66×10^{-1}
120.0	2.17×10^{-1}	119.5	1.21×10^{-1}
122.9	1.63×10^{-1}	122.4	9.40×10^{-2}
125.8	1.16×10^{-1}	125.4	8.10×10^{-2}
128.7	8.24×10^{-2}	128.3	7.28×10^{-2}
131.6	6.52×10^{-2}	131.2	6.93×10^{-2}
134.5	5.72×10^{-2}	134.1	6.77×10^{-2}
137.4	5.83×10^{-2}	137.0	5.99×10^{-2}
140.2	6.44×10^{-2}	142.8	4.51×10^{-2}
143.1	7.40×10^{-2}		

^{52}Cr at 20 MeV		^{62}Ni at 20 MeV	
$\theta_{c.m.}$ (deg)	$(d\sigma/d\Omega)_{c.m.}$ (mb/sr)	$\theta_{c.m.}$ (deg)	$(d\sigma/d\Omega)_{c.m.}$ (mb/sr)
10.58	2.16×10^{4}	10.49	2.99×10^{4}
12.69	1.02×10^{4}	12.59	1.45×10^{4}
15.86	3.13×10^{3}	15.73	4.27×10^{3}
19.03	8.69×10^{2}	18.87	1.23×10^{3}
22.20	4.55×10^{2}	22.01	7.31×10^{2}
25.36	4.14×10^{2}	25.15	5.54×10^{2}
28.52	2.79×10^{2}	28.28	3.13×10^{2}
31.67	1.18×10^{2}	31.41	1.28×10^{2}
34.82	3.54×10	34.54	4.78×10
37.96	2.30×10	37.66	4.95×10
41.10	3.10×10	40.78	5.45×10
44.23	2.79×10	43.89	3.54×10
47.36	1.60×10	47.00	1.57×10
50.48	6.38	50.10	5.54
53.60	3.50	53.19	4.90
56.70	4.66	56.28	6.41
59.80	5.00	59.37	5.56
62.89	3.67	62.45	3.18
65.98	1.59	65.52	1.29
69.05	4.62×10^{-1}	68.58	7.94×10^{-1}
72.12	4.49×10^{-1}	71.64	1.01
75.18	9.01×10^{-1}	74.69	1.11
78.23	1.22	77.73	8.69×10^{-1}
81.27	1.00×10^{-1}	80.76	4.56×10^{-1}
84.30	5.93×10^{-1}	83.79	1.66×10^{-1}
87.32	2.27×10^{-1}	86.81	1.31×10^{-1}
90.34	6.26×10^{-2}	89.82	2.31×10^{-1}
93.34	6.95×10^{-2}	92.82	2.73×10^{-1}
96.34	1.51×10^{-1}	95.82	2.32×10^{-1}
99.32	1.70×10^{-1}	98.81	1.37×10^{-1}
102.3	1.69×10^{-1}	101.8	5.78×10^{-2}
105.3	1.27×10^{-1}	104.8	2.19×10^{-2}
108.2	7.45×10^{-2}		
111.2	3.99×10^{-2}		
114.1	2.85×10^{-2}		

^{64}Ni at 20 MeV		^{90}Zr at 20 MeV	
$\theta_{c.m.}$ (deg)	$(d\sigma/d\Omega)_{c.m.}$ (mb/sr)	$\theta_{c.m.}$ (deg)	$(d\sigma/d\Omega)_{c.m.}$ (mb/sr)
10.47	3.10×10^{4}	10.33	7.88×10^{4}
11.52	2.13×10^{4}	11.37	5.31×10^{4}
12.56	1.45×10^{4}	12.40	3.59×10^{4}
15.70	4.22×10^{3}	15.50	1.24×10^{4}
18.84	1.19×10^{3}	18.60	4.13×10^{3}
21.97	6.41×10^{2}	21.69	1.98×10^{3}
25.10	4.94×10^{2}	24.78	1.21×10^{3}
28.23	3.17×10^{2}	27.88	6.38×10^{2}
31.36	1.21×10^{2}	30.96	2.73×10^{2}
34.48	3.92×10	34.05	1.38×10^{2}
37.59	3.97×10	37.13	1.13×10^{2}
40.71	4.67×10	40.21	8.97×10
43.82	3.34×10	43.29	5.37×10
46.92	1.42×10	46.36	2.82×10
50.02	4.10	49.43	1.86×10
53.11	3.79	52.50	1.67×10
56.19	5.77	55.56	1.35×10
59.28	5.40	58.62	8.37
62.35	3.13	61.67	4.33
65.42	1.16	64.72	2.98
68.48	6.29×10^{-1}	67.76	3.41
71.53	8.68×10^{-1}	73.83	2.71
74.58	1.03	76.86	1.49
77.62	7.81×10^{-1}	79.89	6.76×10^{-1}
80.65	3.61×10^{-1}	70.79	3.61
83.68	1.15×10^{-1}	82.90	4.77×10^{-1}
86.70	1.26×10^{-1}	85.92	6.31×10^{-1}
89.71	2.20×10^{-1}	88.93	7.23×10^{-1}
92.71	2.72×10^{-1}	91.93	6.25×10^{-1}
95.71	2.12×10^{-1}	94.93	3.98×10^{-1}
98.70	1.05×10^{-1}	97.92	2.23×10^{-1}
101.70	3.07×10^{-2}	100.9	1.41×10^{-1}
		103.9	1.27×10^{-1}
		106.9	1.28×10^{-1}
		109.8	1.33×10^{-1}
		112.8	9.92×10^{-2}
		115.8	7.99×10^{-2}
		118.7	6.04×10^{-2}
		121.7	4.44×10^{-2}
		124.6	3.76×10^{-2}

TABLE I (*continued*).

^{116}Sn at 20 MeV $\theta_{c.m.}$ (deg)	$(d\sigma/d\Omega)_{c.m.}$ (mb/sr)
13.34	4.68×10^{4}
15.39	2.47×10^{4}
18.46	9.26×10^{3}
21.54	4.21×10^{3}
24.61	2.26×10^{3}
27.68	1.13×10^{3}
30.75	5.36×10^{2}
33.82	3.21×10^{2}
36.88	2.37×10^{2}
39.94	1.54×10^{2}
43.00	8.58×10
46.06	4.55×10
49.11	3.35×10
52.16	2.85×10
55.21	2.09×10
58.26	1.29×10
61.30	7.85
64.33	5.81
67.37	5.01
70.40	3.93
73.42	2.45
76.45	1.68
79.46	1.39
82.48	1.23
85.49	9.91×10^{-1}
88.49	6.56×10^{-1}
91.50	3.99×10^{-1}
94.49	3.32×10^{-1}
97.49	3.13×10^{-1}
100.5	3.10×10^{-1}
103.5	2.45×10^{-1}
106.4	1.32×10^{-1}
109.4	9.44×10^{-2}
112.4	9.00×10^{-2}
115.4	9.31×10^{-2}
118.3	9.61×10^{-2}
121.3	8.27×10^{-2}
124.3	5.47×10^{-2}
127.2	3.69×10^{-2}

^{62}Ni data in Table II. The χ^2 values shown define R to within $\pm5\%$. We believe that this procedure, which depends on the availability of forward-angle data, substantially reduces the discrepancies in parameter values introduced by uncertainties in the direct calculation of the cross section.[5,6]

The scattering potential used is the standard Woods-Saxon type consisting of the sum of a real well

$$-V\left[1+\exp\frac{r-r_0A^{1/3}}{a}\right]^{-1}, \tag{2}$$

an imaginary well

$$-iW\left[1+\exp\frac{r-r_0'A^{1/3}}{a'}\right]^{-1}, \tag{3}$$

and the Coulomb potential of a uniformly charged sphere of radius $r_{0c}A^{1/3}$. The code allows variation from starting values of any or all of the parameters V, W, r_0, r_0', a, and a', and upon completion of the fit it calculates among other things the total-reaction cross section σ_r. Changing the value of r_{0c} from 1.0 to 1.5 F had a negligible effect on the optical-well parameters; $r_{0c}=1.25$ F was used for all the results reported here. The effect of including a surface-peaked imaginary potential was not investigated. Although in most cases the fits were slightly improved at back angles with the inclusion of a spin-orbit term with form

$$+V_{so}\left(\frac{\hbar}{M_\pi c}\right)^2\boldsymbol{\sigma}\cdot\mathbf{L}\frac{1}{r}\frac{d}{dr}\left[1+\exp\frac{r-r_0A^{1/3}}{a}\right]^{-1}, \tag{4}$$

the resulting values for V_{so} were generally inconclusive.

As in previous studies involving strongly absorbed particles, the present studies displayed a considerable ambiguity between values for the well depths and well radii. There are, of course, certain guidelines which may be employed to limit somewhat this ambiguity and permit the determination of parameters which both provide a good description of the data and to which some physical significance may be attached. These are, in fact, the same guidelines which one uses in studies of

TABLE II. Goodness of fit at forward angles for the 15-MeV ^{62}Ni data. The values of χ^2 presented in the table are for the forward-angle region.

R	$\chi^2(\theta<30°)$
0.95	2.29
1.00	0.36
1.05	0.57
1.10	2.41

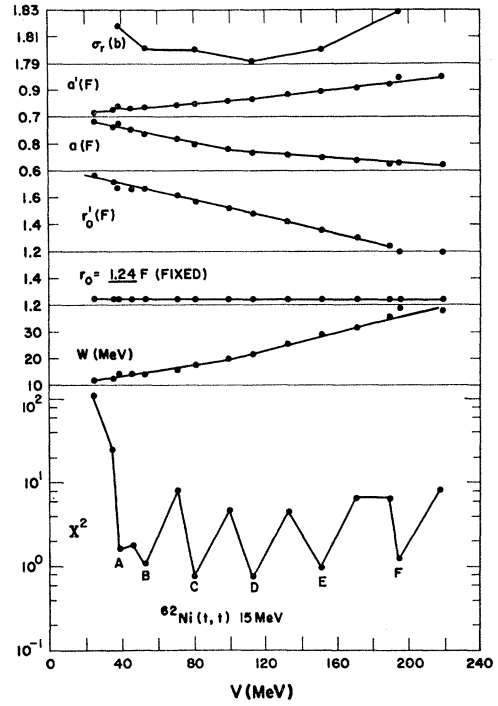

FIG. 1. Various potential families obtained for ^{62}Ni at 15 MeV. The value of r_0 was held fixed at 1.24 F.

[5] J. K. Dickens and F. G. Perey, Phys. Rev. **138**, B1080 (1965).
[6] J. K. Dickens, Phys. Rev. **143**, 758 (1966).

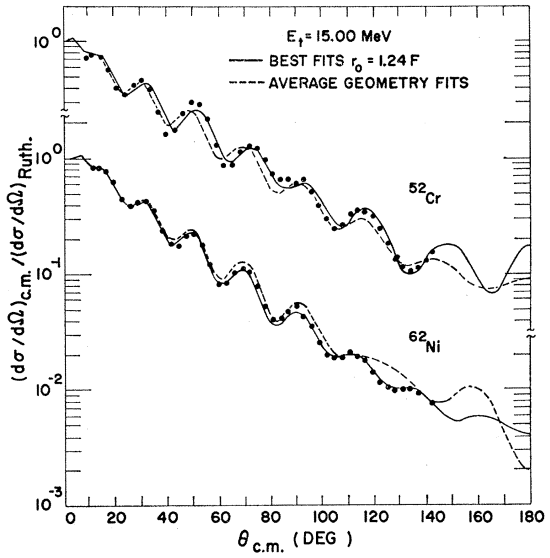

FIG. 2. Optical-model fits to 15-MeV data.

the scattering of the ^{3}He projectile, which, like the triton, is a loosely bound, mass-3, spin-$\frac{1}{2}$ particle. Bassel *et al.*[7] have performed a comprehensive analysis of a variety of ^{3}He data and were able to find a consistent set of parameters which we have used as a basis for the study of the triton data reported here.

In order to suppress the $V(r_0)^n$ degeneracy, a suggestion of Bassel was followed and the real-well radius r_0 was assumed to be approximately the same as for the free nucleon, $r_0=1.24$ F. This assumption is based on the fact that the binding energy of the weakly bound ^{3}He and ^{3}H projectiles is fairly small compared to the real-well depth of the interaction, and, therefore, the nucleons of these projectiles should interact approximately independently in the real well of the scattering potential. Moreover, this choice for r_0 is completely compatible with the data because no other values studied produced better fits to the data, except perhaps for the case of ^{52}Cr where smaller values gave slightly improved fits. Nevertheless, even with this assumption, a large number of families of parameters were still found. As a typical example, Fig. 1 illustrates families of parameters for the 15-MeV ^{62}Ni data. For these results, as for all the fits reported here, r_0 was held fixed at 1.24 F. Each point denoted with a letter in the lower curve of Fig. 1 represents the minimum value of χ^2 found by the search routine for the particular region of parameter space explored. The points between the labeled points are for parameter values intermediate to those for the labeled families and indicate that the families produce definite local minima in the χ^2 space. The values for the parameters are plotted immediately above the corresponding χ^2 value and appear to have an approximately linear dependence on V. The parameter values for the families are listed in Table III. Since all these families give essentially equally good fits, one is not preferred over the other without an additional assumption.

TABLE III. Families of parameters that give good fits to the ^{62}Ni data for 15-MeV incident tritons. The real-well radius r_0 was held fixed at 1.24 F in order to suppress the $V(r_0)^n$ degeneracy. The families A through F are labeled in Fig. 1.

Family	V (MeV)	W (MeV)	r_0' (F)	a (F)	a' (F)	σ_r (b)	χ^2
A	37	14.2	1.67	0.942	0.777	1.82	1.80
B	53	14.0	1.66	0.878	0.766	1.81	1.05
C	80	17.7	1.57	0.795	0.797	1.81	0.78
D	113	22.5	1.48	0.736	0.843	1.79	0.80
E	151	29.0	1.36	0.692	0.890	1.81	1.00
F	194	38.0	1.20	0.651	0.995	1.83	1.48

The assumption employed here follows from the arguments for the choice of r_0; that is, since the nucleons of the triton should interact almost independently with the real well of the scattering potential, the total potential should be approximately three times that of the free nucleon. The usual value of V for nucleons of about 50 MeV leads to a value of about 150 MeV for the triton. Recent theoretical calculations[8] for the case of deu-

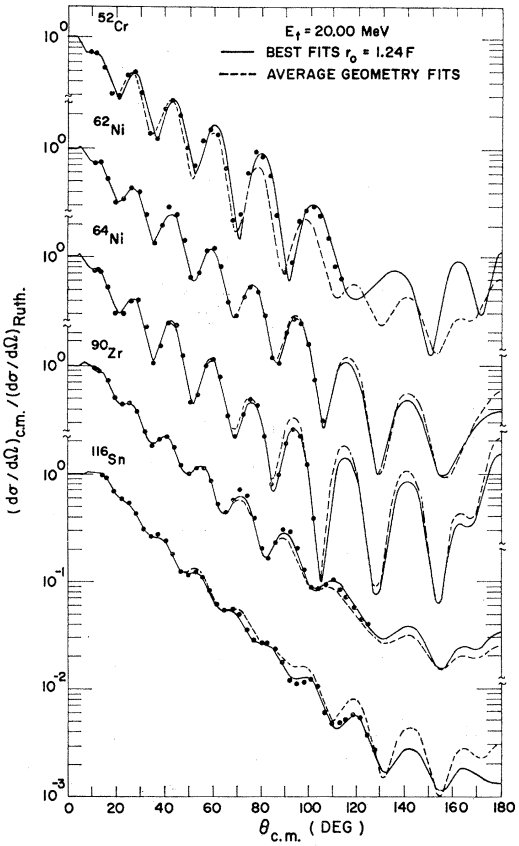

FIG. 3. Optical-model fits to 20-MeV data.

[7] R. H. Bassel, D. D. Armstrong, and A. G. Blair (to be published).

[8] G. Baumgärtner, in Symposium on Recent Progress in Nuclear Physics with Tandems, Heidelberg, 1966 (unpublished).

TABLE IV. Parameters from the "150-MeV" family that give the best fits to the data. The real-well radius was held fixed at $r_0=1.24$ F in order to suppress the $V(r_0)^n$ degeneracy. Except for the case of ^{52}Cr, the fits were not improved by letting r_0 vary along with the other parameters.

Element	E_t (MeV)	V (MeV)	W (MeV)	r_0' (F)	a (F)	a' (F)	σ_r (b)	χ^2
^{52}Cr	15.00	152	22.0	1.49	0.651	0.808	1.68	2.76
^{62}Ni	15.00	151	29.0	1.36	0.692	0.890	1.81	1.00
^{52}Cr	20.00	149	18.8	1.57	0.671	0.776	1.79	2.57
^{62}Ni	20.00	152	26.7	1.43	0.680	0.853	1.91	1.56
^{64}Ni	20.00	154	23.7	1.37	0.672	0.901	1.92	1.56
^{90}Zr	20.00	152	19.6	1.48	0.684	0.771	1.94	1.26
^{116}Sn	20.00	153	20.8	1.42	0.695	0.889	2.12	1.18

terons, in which the real-well depth was determined to be approximately 90 MeV, support this assumption.

A series of parameter searches were carried out with the value of $r_0=1.24$ F and starting with $V=150$ MeV. In these searches, V, W, r_0', a, and a' were allowed to vary until a minimum χ^2 was obtained. The results of this procedure are shown in Table IV and the theoretical predictions given by these parameters are compared to the data in Figs. 2 and 3, the former being for the 15-MeV data and the latter for the 20-MeV data. In general, excellent fits to the data are produced by these parameters over the large range of angles encompassed in the data. The poorest fits occur in the case of ^{52}Cr which represents the only element studied for which the value of $r_0=1.24$ F seems a poor choice. (The best fits for ^{52}Cr were with $r_0=1.10$ F.)

The use of different real and imaginary radii for the potential seems completely justifiable on the basis of both physical arguments and past experience with other projectiles. In particular, for deuteron elastic scattering, different radii are quite necessary to obtain adequate fits to the data.[9] A simplified physical argument for this difference lies in the comparison of the definition for the real and imaginary potentials. As mentioned above, the real potential for each nucleon of the triton is close to that of a free nucleon, whereas the imaginary potential must contain the probability of breakup of the triton which probably occurs at a larger radius and inherently must include the full triton radius. Although this picture of the interaction is certainly oversimplified, it does demonstrate that a larger imaginary radius is physically realistic.

Table IV illustrates that the triton elastic interaction can be well described by a fairly narrow range of parameters over a variety of nuclei. Also listed in this table are the reaction cross sections σ_R as given by the optical-model program for each element. The final column of the table is the final value of χ^2 obtained by the search routine.

Because these results cover only a limited range of nuclides and triton energies, it was considered appropriate to seek an average potential which could be extrapolated to other nuclides. To do this, a simple average of the geometrical parameters given in Table IV was taken and further parameter searches on only V and W were carried out. The results of these fits with average geometrical parameters are summarized in Table V. Graphical comparisons of the theory to the data are also given in Figs. 2 and 3. As might be expected, these fits are not as good as those which included variation of the geometrical parameters, but they nevertheless describe the data fairly satisfactorily. The χ^2 values as given in Table V also indicate the poorer quality of the fit, but they are still quite reasonable. It seems possible to extract a crude dependence of the potential depths upon mass number. Well depths versus atomic-mass number are plotted in Fig. 4, and a linear

TABLE V. Well depths for the "150-MeV" family that give optimum fits to the data with the geometrical parameters held fixed at the average of the values for the best fits.

	$r_0=1.24$ F; $r_0'=1.45$ F; $a=0.678$ F; $a'=0.841$ F				
Element	E_t (MeV)	V (MeV)	W (MeV)	σ_r (b)	χ^2
^{52}Cr	15.00	144	30.0	1.77	7.91
^{62}Ni	15.00	155	21.9	1.76	21.1
^{52}Cr	20.00	146	25.6	1.82	17.2
^{62}Ni	20.00	153	24.7	1.90	2.05
^{64}Ni	20.00	154	20.7	1.89	6.56
^{90}Zr	20.00	151	21.5	2.00	4.03
^{116}Sn	20.00	156	17.4	2.03	14.2

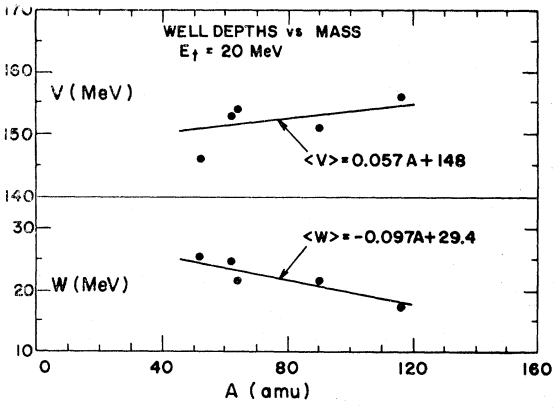

FIG. 4. Real and imaginary potential-well depths as a function of mass number.

[9] R. H. Bassel, R. M. Drisko, G. R. Satchler, L. L. Lee, Jr., J. P. Schiffer, and B. Zeidman, Phys. Rev. **136**, B960 (1964).

TABLE VI. Parameters that give the best fits to the data with $r_0'=r_0$ and $a'=a$.

Element	E_t (MeV)	V (MeV)	W (MeV)	V_{so} (MeV)	r_0 (F)	a (F)	χ^2
^{52}Cr	15.00	22.3	24.2	4.92	1.52	0.736	6.51
^{62}Ni	15.00	29.9	15.8	6.37	1.52	0.714	1.19
^{52}Cr	20.00	25.0	27.6	5.24	1.46	0.777	26.9
^{62}Ni	20.00	28.6	29.3	5.66	1.44	0.791	3.19
^{64}Ni	20.00	32.0	26.7	5.01	1.45	0.779	3.69
^{90}Zr	20.00	29.6	28.0	~0	1.46	0.720	5.87
^{116}Sn	20.00	25.6	17.3	3.92	1.49	0.732	2.64

fit to the potential values produces the following equations:

$$V=(0.057A+148)\text{ MeV},$$
$$W=(-0.097A+29.4)\text{ MeV}.$$

These relations should be considered as approximate because of the scarcity of data available. However, extrapolation to other mass values for incident triton energies near 20 MeV should be reasonably correct and permit more meaningful use of optical-model predictions for other nuclides in this mass region. It was not possible to extract an average energy dependence of the optical-model parameters from the limited number of cases studied.

Finally, Table VI summarizes efforts to produce fits to the data with a minimum number of parameters by setting $r_0'=r_0$ and $a'=a$. As for the cases with unequal radii, we also found in this case families of parameters producing local minima in χ^2 space, but the families with V near 25 MeV gave clearly superior fits compared to families with deeper wells. The values of V and W shown in the table are reminiscent of the early values obtained by Hodgson *et al.*[10] for the scattering of ^{3}He particles. The inclusion of the spin-orbit potential (Table VI) significantly improved the fits and reasonably consistent values for V_{so} were obtained. Inclusion of the spin-orbit potential for the previously considered geometries ($r_0'\neq r_0$, $a'\neq a$) had only slight effects on the fits and consistent values for V_{so} were not obtained.

V. DISCUSSION

The application of the optical-model theory to our triton elastic-scattering data provides a good description of the data. Although we have chosen to emphasize a certain family of parameters ($V\approx 150$ MeV), a large number of families exists for these strongly absorbed particles. It is interesting to consider the effects of such a variety of potentials given in Table III upon the results of DWBA calculations. If there is a considerable effect upon the magnitude and shape of the predictions of DWBA theory as applied to direct interactions, then the ambiguity noted above is indeed not real and only those sets which satisfactorily describe the experimental results of direct interaction investigations should perhaps be used. To investigate such a possibility, the DWBA code JULIE[11] was employed for two distinct types of calculations involving tritons: the $(t,^4\text{He})$ and (t,t') reactions. The results of the $(t,^4\text{He})$ calculations are shown in Fig. 5 where the extreme cases of the real potential-well depth have been used to illustrate the largest possible effects. The figure shows results for the $^{62}\text{Ni}(t,^4\text{He})^{61}\text{Co}$ reaction with parameter sets A and F of Table III; the third curve indicates the effect of the cutoff radius in the DWBA calculation. The ^{4}He-ion potential was the same for all three calculations. Both potentials yield essentially the same angular distribution and differ in magnitude by less than 20%. This variation in strength is indeterminate in selecting one potential over another, since the spectroscopic factors remain uncertain to within 20%–30%. Figure 6 shows predictions for the $^{64}\text{Ni}(t,t')^{64}\text{Ni}$ reaction to the 1.34-MeV 2^+ state for three potential sets; two of the sets correspond to the extreme cases considered above (sets A and F), and the third set (set E) is the one which has been argued above to have the preferred well depth. As in Fig. 5, the predictions are plotted in arbitrary units of magnitude, but with the correct relative strengths. The JULIE calculation was also performed

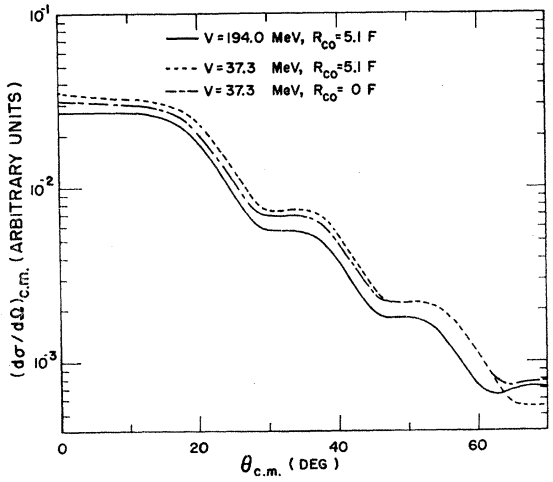

FIG. 5. $^{62}\text{Ni}(t,^4\text{He})^{61}\text{Co}$ DWBA calculations for the $l=3$, ground-state transition with different families of parameters for the triton channel. The effect of a cutoff radius is also indicated.

[10] P. E. Hodgson, Nucl. Phys. **21**, 28 (1960); **23**, 499 (1961).

[11] R. M. Drisko (unpublished); and Oak Ridge National Laboratory Report No. ORNL 3240 (unpublished).

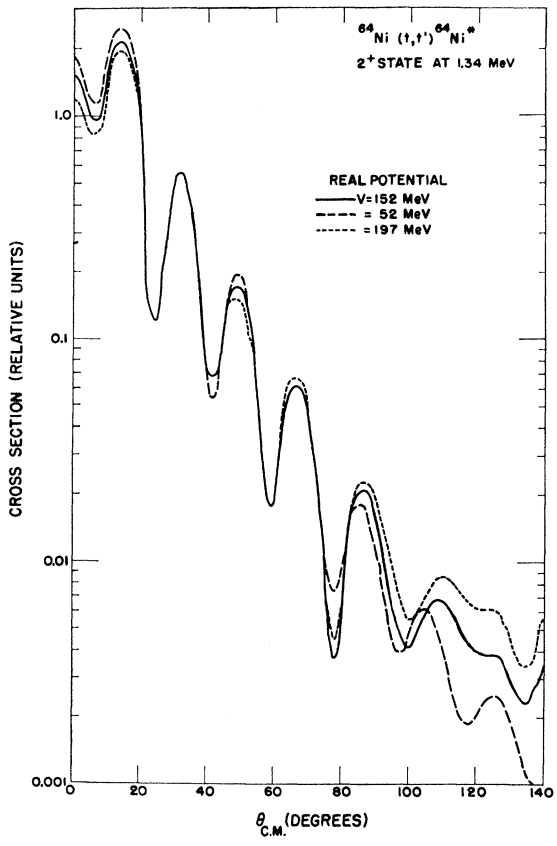

FIG. 6. ^{64}Ni$(t,t')^{64}$Ni* DWBA calculations for the first excited (2^+) state of ^{64}Ni.

under the condition that the excitation of the 2^+ level can be described as a vibrational excitation requiring the use of a complex form factor, as has been found necessary for other strongly absorbed particles.[12] Again, the shapes of the predicted angular distributions are not very different, except for slight effects at large angles. Also, the magnitudes are nearly the same, and, since the deformation parameter is proportional to the square root of the ratio of the predicted cross section to the measured cross section, again it would be difficult to establish the correctness of any one set of parameters. There is, however, an indication from preliminary studies at the Laboratory that the 150-MeV family does provide a better backward-angle fit to inelastic-scattering data.

It is not unexpected that the DWBA calculations are rather independent of the optical-potential family chosen for the triton. The triton is a strongly absorbed particle and has a small mean free path inside the nucleus. Thus the wave function need be described only over a small region at the surface. Any potential which can generate the required wave function over this localized region will then give the correct elastic scattering and the necessary distorted waves for the DWBA calculation.

In contrast to the above results, there has been some work on double stripping such as (t,p) reactions which indicate that this mechanism is sensitive to the choice of triton potential.[13,14] It was found that the best comparisons to the experimental data were obtained with a real potential of three times the free proton or neutron potential. This result is in agreement with the preferred choice mentioned above, although the reasons for the sensitivity in this case are not clear.

An interesting feature of the general results of the present optical-model study of triton elastic scattering is the somewhat smaller imaginary radii obtained as compared to those for ^{3}He scattering. The present analysis produces an average imaginary radius of 1.45 F, whereas similar analysis of ^{3}He-elastic scattering data[7] yields almost 1.6 F. The strong-absorption model of Frahn and Venter[15] when applied to these data also gives a difference in absorption radii of approximately the same magnitude as that observed for the optical model. As a result of this behavior the difference between predictions of DWBA calculations of inelastic scattering with a real form factor and a complex form factor is less in the case of tritons than in the case of the ^{3}He particle.[12] The different imaginary radii produce this effect, since more of the real potential enters into the interaction in the case of the triton. The explanation for a smaller imaginary radius parameter for the triton probably lies in the isotopic-spin dependence of the interaction. No attempt to explore a dependence of the parameters on the isotopic spin of the projectile has been attempted here.

ACKNOWLEDGMENTS

It is a pleasure to acknowledge the efforts of Dr. D. D. Armstrong throughout this program and also the numerous suggestions of Dr. R. H. Bassel. Without the work of J. Levin and W. S. Hall, the use of the on-line computer would have been impossible. Finally, the crew of the Los Alamos tandem Van de Graaff is to be complimented on the excellent triton beams furnished for these experiments.

[12] E. R. Flynn and R. H. Bassel, Phys. Rev. Letters **15**, 168 (1965).

[13] R. N. Glover and A. D. W. Jones, Phys. Letters **18**, 165 (1965).

[14] R. M. Drisko and F. Rybicki, Phys. Rev. Letters **16**, 275 (1965).

[15] W. E. Frahn and R. H. Venter, Ann. Phys. (N. Y.) **27**, 135 (1964).